13th International Symposium on Particle Image Velocimetry – ISPIV 2019
Munich, Germany, July 22-24, 2019

Simultaneous measurements of velocity and temperature fields in large aspect ratio Rayleigh-Bénard convection

Sebastian Moller*, Alexander Thieme, Christian Resagk, Christian Cierpka

Technische Universität Ilmenau, Institute of Thermodynamics and Fluid Mechanics, Ilmenau, Germany

*sebastian.moller@tu-ilmenau.de

Abstract

In this contribution, simultaneous measurements of velocity and temperature fields in horizontal planes in Rayleigh-Bénard convection are anaylzed. The investigations were performed in a water filled Rayleigh-Bénard cell with dimensions of $l \times b \times h = 700\,\mathrm{mm} \times 700\,\mathrm{mm} \times 28\,\mathrm{mm}$ and, therefore, a large aspect ratio of $\Gamma = l/h = 25$, so that the experimental results can be compared to already existing numerical results. Thermochromic Liquid Crystals (TLCs), which appear in different colors in dependency of their temperature when illuminated by white light, are used for the measurements, thereby enabling the use of Particle Image Velocimetry (PIV) for the velocity field measurements, while the temperature field is determined via their color signal. The uncertainty of temperature measurement is analyzed, especially with respect to a large field of view and accordingly a wide range of viewing angles, affecting the color signal of TLCs. Concerning the whole field of view, a mean measurement uncertainty in the range of $0.15\,\mathrm{K}$ is achieved, offering the possibility to detect small temperature differences in Rayleigh-Bénard convection precisely. The measurements within a horizontal plane in close vicinity to the cooling plate of the Rayleigh-Bénard cell clearly demonstrate the emergence of convective flow patterns, which are explained by means of the velocity and temperature field. Finally, a comparison between numerical results and the results obtained here is shown and discussed.

1 Introduction

As thermal convection is one of the most frequent flow types in nature, it has already been analyzed by means of experiments and simulations for many years. However, a lot of questions still remain open. Among these are the correlation between the transport of heat and momentum in thermal convection and the spatial and temporal scaling of coherent structures, so-called superstructures, see Pandey et al. (2018) and Fonda et al. (2019). A canonical experiment used for the investigation of thermal convection is the Rayleigh-Bénard experiment, which consists of an enclosed fluid volume that is heated from below and cooled from above, thereby inducing thermal convection. In particular, the physics of Rayleigh-Bénard systems with a large aspect ratio $\Gamma = l/h$ between the lateral dimension l and height h of the cell is of major interest, as these represent typical natural systems as for example the atmosphere. Despite their importance such systems have not been studied in great detail so far. Therefore, the current study is focused on large aspect ratio Rayleigh-Bénard convection and aims for simultaneous measurements of velocity and temperature fields. This enables to gain detailed insights into the correlation between the transport of heat and momentum, which is the key to the understanding of the local heat flux. For simultaneous measurements of the velocity and temperature field, different optical measurement techniques have been proven to be successful in the past. On the one hand, common tracer particles can be used for the determination of the velocity field with Particle Image Velocimetry (PIV), while a luminescent dye is dissolved in the fluid additionally and illuminated with light of a certain wavelength, in order to estimate the temperature field via the intensity or lifetime of luminescene, see Massing et al. (2016) and Massing et al. (2018). On the other hand, particles doped with temperature sensitive dyes or rare-earth ions can be applied to measure the velocity and temperature field simultaneously, investigated by Fond et al. (2012). Another approach is the use of Thermochromic Liquid Crystals (TLCs), which appear in different colors in dependency of their ambient temperature when illuminated with white light, see Schmeling et al. (2014) and Segura et al. (2015). Hence, evaluating the motion of TLCs with PIV

and analyzing their color appearance enables simultaneous measurements of velocity and temperature fields, too. Furthermore, TLCs offer the possibility to measure temperatures over small temperature ranges very precisely, predestining them for applications, which require the analysis of small temperature differences. Therefore, TLCs in water as the working fluid are used in the present case. However, the color appearance of TLCs also strongly depends on the angle between observation and illumination, affecting the range as well as the uncertainty of temperature measurement shown by Moller et al. (2019). This effect has to be taken into account in the calibration of the temperature measurement, especially when observing a large field of view with a wide range of angles between observation and illumination, what is demonstrated here at an exemplary measurement in a horizontal plane of a Rayleigh-Bénard cell.

2 Experimental setup

In order to investigate thermal convection at large aspect ratios, a Rayleigh-Bénard setup for applying water as the working fluid was built up. This setup enables to use Rayleigh-Bénard cells with different heights and a squared bottom area of $700\,\mathrm{mm} \times 700\,\mathrm{mm}$. Three cells with a varying height have been set up so far, yielding aspect ratios $\Gamma = l/h$ of $\Gamma = 10$, $\Gamma = 20$ and $\Gamma = 25$. In order to ensure the accessibility for optical measurement techniques like for example PIV, the side walls and the cooling plate at the top are made of glass. The top plate is cooled by water flowing above it in a separate circuit, which is covered by a second glass plate for the optical access, as schematically shown on the left side of figure 1. In the design of the separate circuit for the cooling water many aspects had to be considered. In particular, the thickness of the glass plates, the flow rate of the cooling water and the geometry of the flow guiding elements in close vicinity to these plates had to be chosen advisedly to reach a homogeneous temperature distribution on the cooling plate of the Rayleigh-Bénard cell as well as a safe operation mode.The heating plate at the bottom is made of aluminium, ensuring a homogeneous temperature distribution at its surface, which is anodized to be persistent. The temperature of this plate is controlled by water flowing through meander channels within the plate. Furthermore, the setup is equipped with several sensors to measure the temperature of the heating and cooling plate as well as of the cell's side wall. Both the heating and cooling water circuit are connected to temperature control units with high power to provide the required heat transfer for the Rayleigh-Bénard cell. However, the maximal temperature difference between the heating and cooling plate is limited because of the large temperature drop over the cooling plate in direction of its thickness, due to the low heat conductivity of glass. Therefore, the water in the cooling circuit has to be at considerably lower temperature than the desired cooling plate temperature inside the Rayleigh-Bénard cell. Nevertheless, temperature differences up to $\Delta T = 10\,\mathrm{K}$ and consequently an extended range of Rayleigh numbers can be achieved. The Rayleigh number Ra is defined as $Ra = \alpha g \Delta T h^3/(\nu\kappa)$ with the thermal expansion coefficient α, acceleration due to gravity g, kinematic viscosity ν and thermal diffusivity κ. Considering all three aspect ratios, the obtainable Rayleigh numbers are in between $Ra \in [10^5, 10^8]$.

For measuring the temperature fields in the Rayleigh-Bénard cell via the color of the TLCs, a color camera (sCMOS PCO edge 5.5, PCO AG) with a Bayer filter is applied for color recording. The camera is equipped with a wide-angle lens (Zeiss Otus 1.4/28, Carl Zeiss AG), in order to observe a large field of view. Furthermore, a tild adapter between the color camera and objective lens is used to take the Scheimpflug condition into account, due to the non-perpendicular observation of the measurement plane, which will be explained in the following section. The experimental setup with the color camera as well as the white light source for the illumination of the TLCs is depicted on the right side of figure 1.

Since the TLCs must be illuminated by white light to show different colors in dependency of their temperature, a common laser emitting a single fixed wavelength can not be used for the illumination. Therefore, white LEDs in combination with a special light sheet optics according to Schmeling et al. (2014) are used to shape a white light sheet covering the cell's whole cross-sectional area of $700\,\mathrm{mm} \times 700\,\mathrm{mm}$. In order to cope with the nature of the light emitted by the LEDs, which are arranged horizontally along a line, small lenses are clipped on each LED, reducing the divergence of the light drastically. Furthermore, the light passes through a slit aperture and is focused by Fresnel lenses to obtain uniformity regarding the thickness of the light sheet. By adapting the width of the slit aperture and the distance between the LEDs, slit aperture and Fresnel lenses, a light sheet with a thickness of less than 5 mm over the whole cross section of the cell and high light intensity can be achieved. A sketch and a picture of the interior of the light source for the illumination of the TLCs in horizontal planes of the Rayleigh-Bénard cell can be seen in figure 2.

In this case, TLCs of type R20C20W (LCR Hallcrest), which nominally start to show a red color at $T = 20\,^\circ\mathrm{C}$ and pass through the whole visible spectrum until they appear blue at $T = 40\,^\circ\mathrm{C}$, were used for the investigation of the temperature field. It should be emphasized, that this specification only applies to

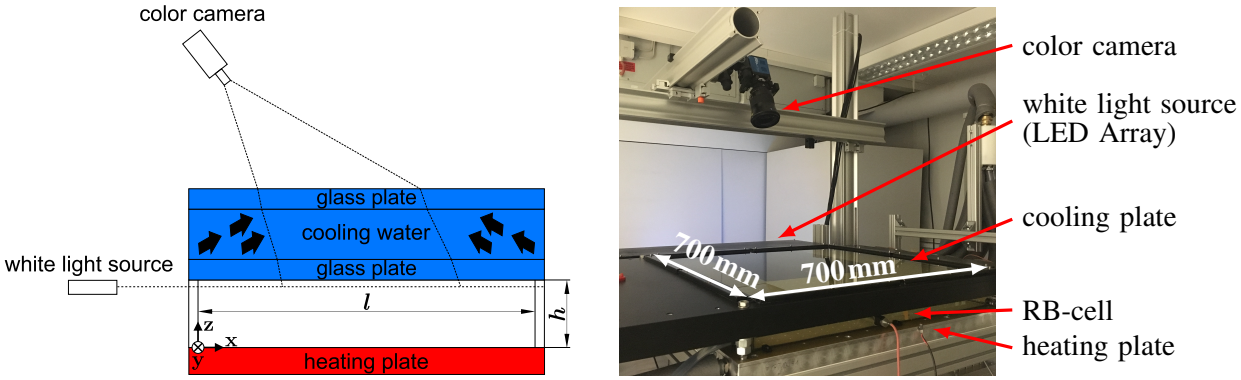

Figure 1: Sketch of the the experiment (left) and real experimental setup (right) for simultaneous velocity and temperature field measurements in horizontal planes of the Rayleigh-Bénard (RB) cell. The picture on the right side shows the Rayleigh-Bénard cell with aspect ratio $\Gamma = 25$. It is noted, that the coordinate system in the left corner of the sketch is valid for all of the following investigations.

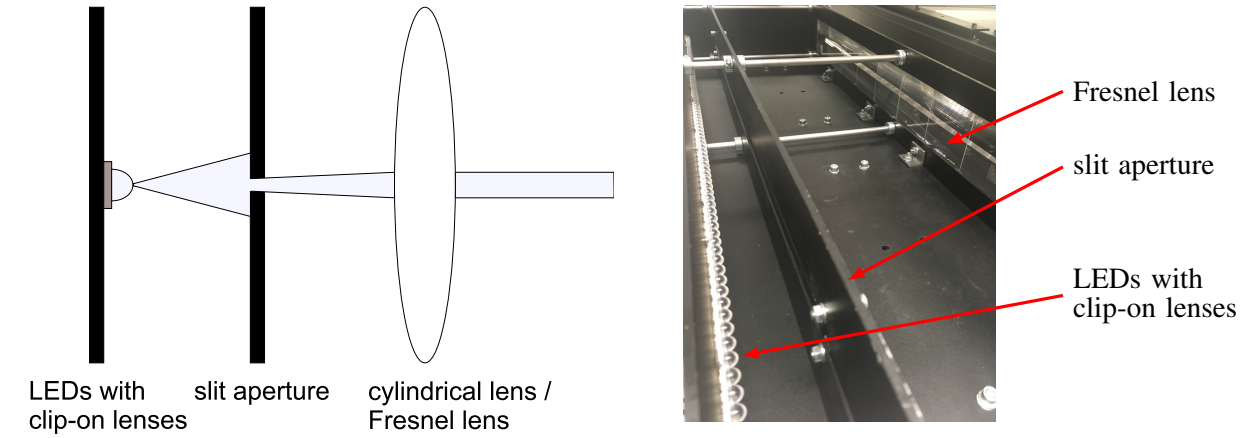

Figure 2: Sketch of the light sheet optics (left) and the interior of the light source (right) for the generation of a white light sheet.

the case, that illumination and observation are done from the same direction. However, if the angle between illumination and observation is changed, the specifications differ strongly. Especially, if the color camera and light sheet are arranged perpendicularly, the main color change of TLCs passes much faster, leading to a higher sensitivity and, therefore, lower uncertainty of temperature measurement at the expense of a reduced measurement range. Thus, the angle between illumunation and observation always has to be considered regarding the temperature measurement range and, if possible, should be adapted resulting in strong color variations over the whole range according to Moller et al. (2019).

3 Experimental conditions and procedure

In order to show simultaneous measurements of velocity and temperature fields in large aspect ratio Rayleigh-Bénard convection, the cell with aspect ratio $\Gamma = 25$ and dimensions of $l \times b \times h = 700\,\text{mm} \times 700\,\text{mm} \times 28\,\text{mm}$ was used in this case. As the most distinctive structures in the velocity and temperature field occur in close vicinity to the isothermal plates, a horizontal plane close to the cooling plate of the Rayleigh-Bénard cell was chosen for the measurements, so that the benefit of using TLCs can be illustrated clearly. More precisely, a white light sheet with a thickness of about 3 mm, generated with the light source described above, was shaped over the whole cross-sectional area of the cell, reaching from $z = 24\,\text{mm}$ to $z = 27\,\text{mm}$ in

direction of the cell's height when measured from the surface of the heating plate at $z = 0\,\mathrm{mm}$. Since direct numerical simulations have been performed by Fonda et al. (2019) for the aspect ratio $\Gamma = 25$, the results can directly be compared to each other. For ensuring the comparability, two more dimensionless numbers in terms of the Rayleigh number and Prandtl number must be as equal as possible. Fonda et al. (2019) varied the Rayleigh number for a fixed Prandtl number of $Pr = 7$ in their simulations. Since water with $Pr \approx 7$ was used for the experiments considered in this study, the Prandtl number is the same as in the simulations. The Rayleigh number, which is chosen for comparison, is $Ra = 10^6$, as this is the most appropriate one for the experimental realization with respect to the temperature difference between heating and cooling plate. However, the required temperature difference for $Ra = 10^6$, which amounts to about $\Delta T = 3.3\,\mathrm{K}$ in this case, is too large for observing the TLCs using the common PIV-setup, meaning to record the color signal of the TLCs for an angle of $\varphi = 90^\circ$ between illumination and observation. According to Moller et al. (2019), the temperature range of color play of the TLCs decreases drastically for $\varphi = 90^\circ$, so that the occuring temperatures could not be measured over the whole range in this case. Hence, the angle between illumination and observation was adapted to $\varphi = 70^\circ$, as this angle offers precise temperature measurements over a larger range than the perpendicular setup.

Since the application of PIV for the velocity measurements is state of the art, the focus is on the temperature measurements via the color appearance of TLCs. In order to get the correlation between the color and temperature of the TLCs, a calibration measurement in the horizontal plane underneath the cooling plate was performed initially. For this, the water in the cell was cooled down to about $T = 18\,^\circ\mathrm{C}$ and images of the TLCs were recorded with the color camera for different isothermal states in the cell up to $T = 22.3\,^\circ\mathrm{C}$. This temperature range was chosen with regard to the following measurements of Rayleigh-Bénard convection, which require a temperature difference between heating and cooling plate of about $\Delta T = 3.3\mathrm{K}$ for a Rayleigh number of $Ra = 10^6$. Thus, the required temperature difference is covered by the calibration measurements assuredly. Moreover, the absolute position of the temperature range was adapted to the color play of the TLCs, which should be as strong as possible for a low uncertainty of temperature measurement. For ensuring a uniform temperature distribution in the whole cell for each recording of the calibration measurement, the temperature of the heating and cooling plate were matched and at least thirty minutes were waited after adjusting each temperature step, respectively. Furthermore, the uniformity of temperature was abetted strongly by forced convection, which was induced by a hand pump connected to a small hole in one of the sidewalls over a tube, which is used for filling the water into the cell, too. The pressure applied to the handpump was equalized through a second hole in another sidewall, thereby enabling to mix the water in the cell. One hundred single frame images were recorded with a frequency of $f = 5\,\mathrm{Hz}$ for each temperature step, in order to achieve a reliable calibration. However, not the whole cross-sectional area of the cell was recorded, but a central section with lateral dimensions of about $l_x \times l_y = 350\,\mathrm{mm} \times 300\,\mathrm{mm}$, which corresponds to $l_x \times l_y = 12.5\,h \times 10.7\,h$, yielding enhanced spatial resolution.

Velocity and temperature fields in the central section of the Rayleigh-Bénard cell were simultaneously measured for temperatures of $T_h = 21.5\,^\circ\mathrm{C}$ at the heating plate and $T_c = 18.2\,^\circ\mathrm{C}$ at the cooling plate. Therefore, all the occuring temperatures are within the calibrated range. The velocity fields were evaluated using a planar PIV-algorithm, so that the in-plane velocity components are determined in this case. The calibration measurements for PIV were performed with an equidistant grid on the surface of the heating plate. Although the measurement plane is underneath the cooling plate, the calibration is valid in good approximation, due to the small distance between heating plate and measurement plane in comparison to the distance from the measurement plane to the camera, which amounts to about $0.7\,\mathrm{m}$. Furthermore, small deviations regarding the calibration for PIV can be accepted here, as the focus is not on highly accurate velocity measurements, but on a first comparison to the results obtained in Fonda et al. (2019) and on showing the possibility of simultaneous measurements of velocity and temperature fields over a large field of view using TLCs.

4 Results

In the following section, the use of TLCs for temperature measurements is characterized with respect to their color appearance in dependency of the temperature as well as of the observation angle. Furthermore, uncertainty analysis for this temperature measurement technique are performed, in order to assess its applicability for measurements over a large field of view. Finally, the potential of TLCs is shown at simultaneous measurements of velocity and temperature fields in large aspect ratio Rayleigh-Bénard convection, which are compared to numerical results.

4.1 Characterization of the temperature measurement technique

For the calibration of the temperature measurements, the correlation between the color appearance of the TLCs and their temperature was investigated in detail. However, as outlined above, the color of TLCs does not only depend on the temperature, but on the angle between illumination and observation, too. Therefore, the color appearance of TLCs also changes within the field of view due to a varying angle, even though the temperature is constant. This is exemplarily demonstrated in figure 3, which shows snapshots of the TLCs for three different temperatures. Despite the respective uniform temperature distributions in the whole cell, a distinct color play from the left to the right end can clearly be seen. In order to take this effect into account in the temperature measurements, a two-dimensional calibration approach is used, meaning that the whole field of view is split into many interrogation windows with separate calibration curves. In the following, these curves are discussed at the example of three different interrogation windows, which are marked in the snapshots in figure 3 with yellow squares, respectively.

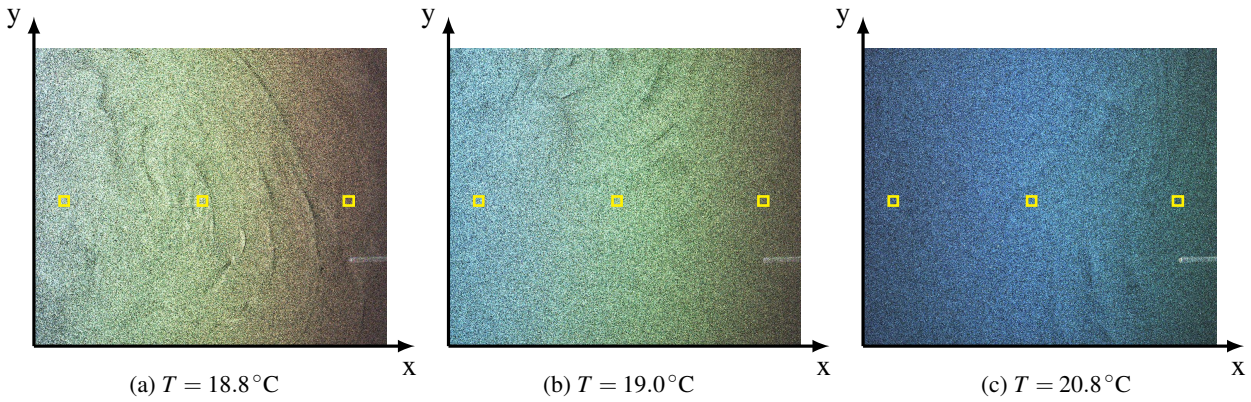

(a) $T = 18.8\,^{\circ}\mathrm{C}$ (b) $T = 19.0\,^{\circ}\mathrm{C}$ (c) $T = 20.8\,^{\circ}\mathrm{C}$

Figure 3: Snapshots of the TLCs R20C20W for three different temperatures. The yellow rectangles indicate the interrogation windows with a size of 32×32 Pixel, which are considered regarding the color signal of the TLCs in dependency of the temperature. The TLCs are illuminated from the left side, which is indicated by the coordinate system corresponding to figure 1.

For the characterization of the color of the TLCs in different interrogation windows, the intensity of the red (R), green (G) and blue (B) channels, given by a camera internal algorithm for each pixel, have to be evaluated. In the first step, all the values for each intensity were averaged over all pixels of one interrogation window, respectively. Next, the mean values for the red, green and blue intensity were transformed into the colorspace of Hue (H), Saturation (S) and Value (V). In this colorspace, Hue represents the color shade in terms of an angle ranging from $H \in [0^{\circ}, 360^{\circ}]$, which is normalized here, so that $H \in [0,1]$. The Saturation indicates, if the color is more pure ($S = 1$) or white ($S = 0$), while the Value quantifies the intensity of the signal with $V \in [0,1]$. Using the HSV-colorspace instead of the RGB-colorspace enables to consider only one scalar for the evaluation of the temperature of the TLCs, which is the value of Hue that shows a strong dependency of the temperature. Furthermore, the value of Hue is not affected by the seeding density of the TLCs and the light intensity of illumination, making the temperature calibration more robust. Therefore, evaluating the value of Hue is suitable for temperature measurements via the color of TLCs, which is why only Hue is taken into account in the following. The value of Hue for each temperature step and interrogation window is averaged over all the 100 snaphots in time t, in order to get a calibration curve $\langle H \rangle_t(T)$ for each interrogation window.

The exemplary calibration curves for the interrogation windows marked in figure 3 are depicted in figure 4. It can be seen that the dynamic range of Hue reaches from nearly $H = 0$ up to about $H = 0.6$ in the given temperature range from $T = 17.9\,^{\circ}\mathrm{C}$ to $T = 22.3\,^{\circ}\mathrm{C}$, corresponding to a color change from red to blue. Furthermore, this figure clearly demonstrates the dependency of the color appearance of TLCs on the position within the field of view, due to a varying angle between illumination and observation. While the color in terms of Hue changes faster at low temperatures for larger observation angles at the left side, the color changes more gradually with temperature for smaller observation angles towards the right side of the field of view. Additionally, the red marked minimum of the curves and, therefore, the temperature corresponding to the red start of the TLCs is shifted to larger temperatures towards the right side of the cell with decreasing observation angle. Since temperatures can only be measured in the range from the minimum

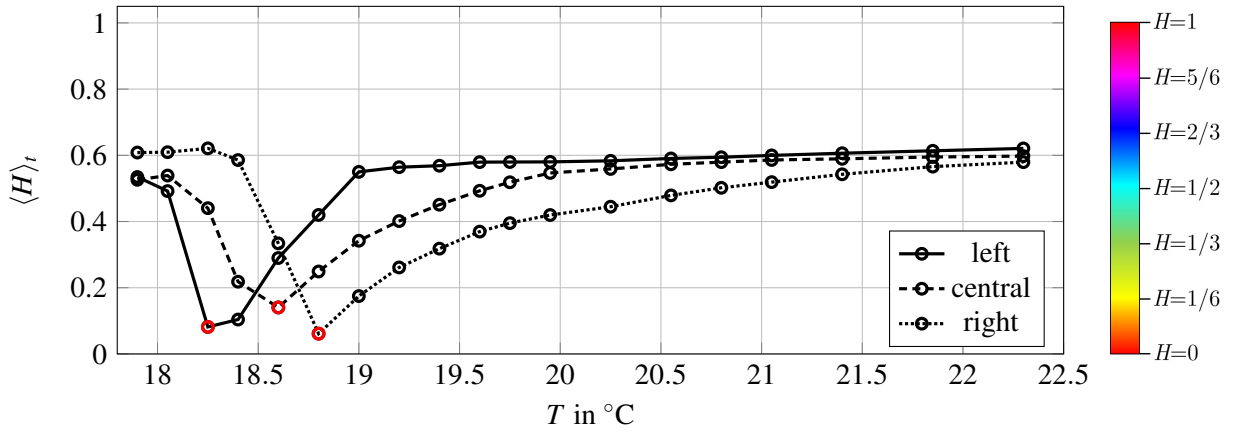

Figure 4: Color appearance of the TLCs R20C20W in terms of Hue in dependency of the temperature for three interrogation windows in the field of view, which are marked in 3. For a better illustration, the colorbar on the right side shows the change of color appearance with Hue. The red markers at the minimum of each curve indicate the onset of the investigated temperature range with unambiguous correlation to the color appearance of the TLCs, respectively.

upward due to ambiguity, the measurable temperature range varies slightly within the field of view, too. In this case, the occuring temperatures should not be smaller than $T = 18.8\,^{\circ}\mathrm{C}$, which is the limiting minimum, corresponding to the calibration curve of the interrogation window at the right end of the cell.

As the slope of Hue with temperature affects the uncertainty of temperature measurement, the uncertainty also depends on the position inside the field of view due to varying observation angles, see König et al. (2018) and Moller et al. (2019). In order to estimate the uncertainty, all of the 100 images for each temperature step are used to calculate the temperature T_{calc} for each interrogation window based on its calibration curve $\langle H \rangle_t (T)$ using linear interpolation. The mean deviation of the calculated temperatures to the set value of the calibration over the whole area A and time t as well as the corresponding standard deviation as an error bar can be seen in figure 5. According to the measurable temperature range, only temperatures $T > 18.8\,^{\circ}\mathrm{C}$ are considered. From this figure, it is obvious that the TLCs R20C20W enable precise temperature measurements in the given range. In particular, for temperatures $18.8\,^{\circ}\mathrm{C} \leq T \leq 19.6\,^{\circ}\mathrm{C}$ the standard deviation does not exceed $\sigma_{T_{calc}} = 0.1\mathrm{K}$, while the mean deviation of the calculated temperatures to the set value of calibration is negligible. For larger temperatures up to about $T < 21.4\,^{\circ}\mathrm{C}$ the standard deviation mainly ranges between $0.1\,\mathrm{K} < \sigma_{T_{calc}} < 0.25\,\mathrm{K}$ and the mean deviation of T_{calc} is still negligible. However, if the temperature increases up to $T > 22\,^{\circ}\mathrm{C}$, it can not be measured precisely anymore, as the mean deviation of the calculated temperatures amounts to larger values. This is due to the fact, that the color appearance of the TLCs does not change to a considerable extent for those temperatures, leading to a fall off in quality of the temperature measurements.

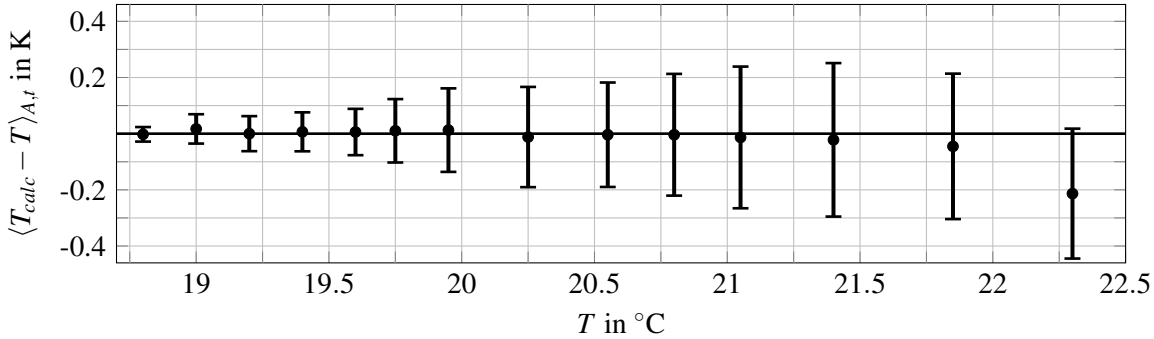

Figure 5: Mean deviation of the calculated temperatures to the set value of calibration over the whole area A and time t with error bars showing the standard deviation of the calculated temperatures.

4.2 Velocity and temperature field measurements in Rayleigh-Bénard convection

Measurements of the velocity and temperature field in Rayleigh-Bénard convection were performed, applying the experimental conditions outlined in section 3. For this, the temperature of the heating and cooling plate were set to $T_h = 21.5\,^{\circ}\mathrm{C}$ and $T_c = 18.2\,^{\circ}\mathrm{C}$, respectively, resulting in a Rayleigh number of about $Ra = 10^6$. Flow structures in the horizontal measurement plane in close vicinity to the cooling plate can be observed clearly in figure 6a, which shows an instantaneous image of the TLCs. These flow structures organize themselves in patterns, which evolve over the whole cross-sectional area with different size and shape. Without any regard to quantitative investigations of the velocity and temperature field, the color of the TLCs already reveals their emergence. Warm fluid upwelling in the center of each pattern, due to its reduced density, streams outwards in the vicinity of the cooling plate, hits the fluid of an adjacent pattern and flows down again with decreased temperature resulting from the heat loss to the cooling plate. However, for further investigations concerning the influence of the patterns on the nature of Rayleigh-Bénard convection, it is necessary to analyze the temperature and velocity field, especially with regard to the local heat flux. In order to determine the temperature field based on the color of the TLCs, the image is initially split into interrogation windows of 32×32 pixel corresponding to about $4\,\mathrm{mm} \times 4\,\mathrm{mm}$ in size. For each interrogation window, the color is characterized in terms of Hue, leading to the Hue field $H(x,y)$ shown in figure 6b. According to the calibration approach described above, the temperature field in figure 6c was calculated based on the calibration curves relating to the interrogation windows by linear interpolation of Hue. Both, the Hue field and temperature field clearly represent the flow patterns of figure 6a, too. Furthermore, the temperature field confirms the mentioned principle of the pattern's emergence, as it shows the warm fluid in the center of each pattern and cold fluid at its rim. The velocity field in figure 6d, which was computed using a standard planar PIV-algorithm, also verifies this behaviour, since locations of warmer fluid come along with sources, while locations of colder fluid are attended by sinks. Moreover, the contour plot in the background of figure 6d represents the absolute value of the horizontal velocity U, demonstrating low values at the sources and sinks, because the fluid mainly streams upward or downward. In comparison, the horizontal velocities are larger in between the center and the outline of each pattern, where the flow direction is basically parallel to the cooling plate.

In order to compare the experimental results with those obtained from simulations in Fonda et al. (2019), the time averaged velocity and temperature fields in Rayleigh-Bénard convection at $Ra = 10^6$ are considered. The averaging of the simulation data was also performed over the same area in direction of the cell's height, which is covered by the light sheet in the experiments, to ensure the comparability. Furthermore, the results are normalized for comparison according to $\tilde{x} = x/h$ and $\tilde{y} = y/h$ for the length scales as well as $\tilde{t} = t/t_f$ with the free-fall time $t_f = \sqrt{h/(\alpha g \Delta T)}$ for the time scales. For the normalization of the absolute value of the horizontal velocity U, the free-fall velocity $u_f = \sqrt{\alpha g \Delta T h}$ is used and yields $\tilde{U} = U/u_f$, while the temperatures are normalized with the heating and cooling plate temperatures using $\tilde{T} = (T - T_c)/(T_h - T_c)$. The results for the time averaged temperature and velocity fields are opposed to each other in figure 7. The experimental data were recorded over a time span of $t = 200\,\mathrm{s}$, resulting in an averaging time of 95 free-fall times, as the free-fall time amounts to about $t_f = 2.1\,\mathrm{s}$ in this case. For direct comparability the numerical results were averaged over 95 free-fall times, too.

In comparison to the temperature field of the instantaneous snaphsot shown in figure 6c, the small-scale patterns are nearly removed after averaging. However, the existence of large-scale patterns, the so-called superstructures, covering dimensions which are considerably larger than the height h of the cell, is revealed in the mean temperature field depicted in figure 7a. These superstructures can also be seen in the time-averaged temperature field obtained by simulations of Fonda et al. (2019). Corresponding to the temperature fields, the time-averaged velocity fields of the experimental data and simulations in figure 7c and 7d visualize the superstructures, too. Their boundaries are represented by low horizontal velocities, which result from the sources and sinks according to the temperature field. Hence, the emergence of superstructures is shown by both the experimental and numerical results in a similar manner, confirming the achieved results.

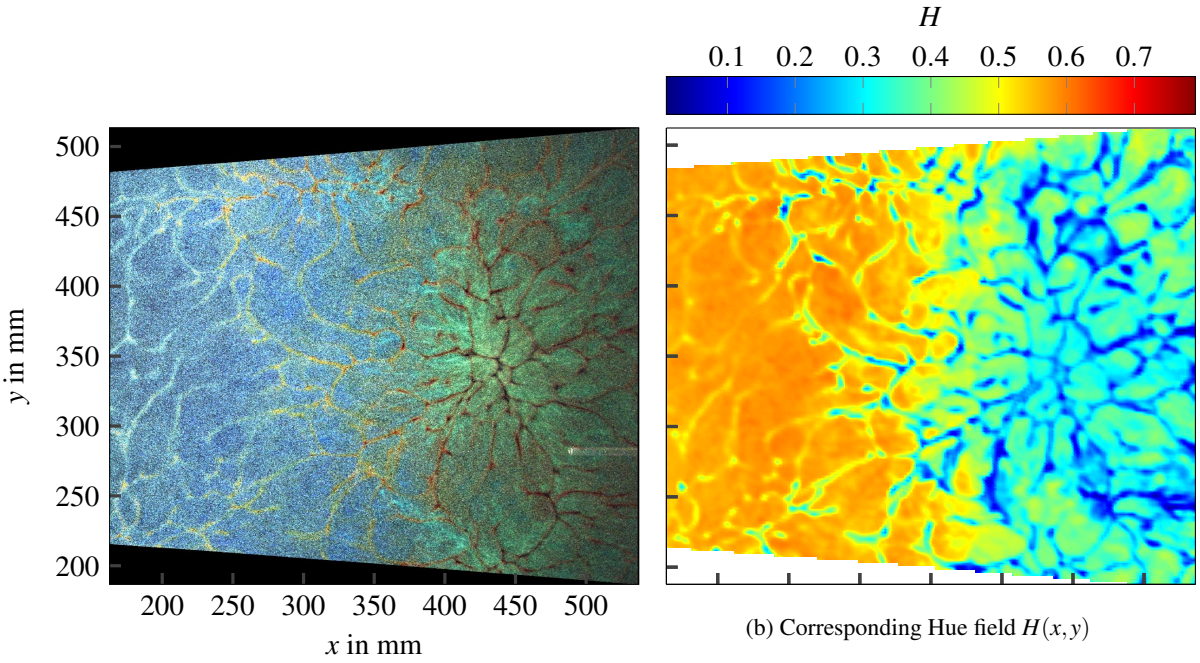

(a) Instantaneous image of TLCs

(b) Corresponding Hue field $H(x,y)$

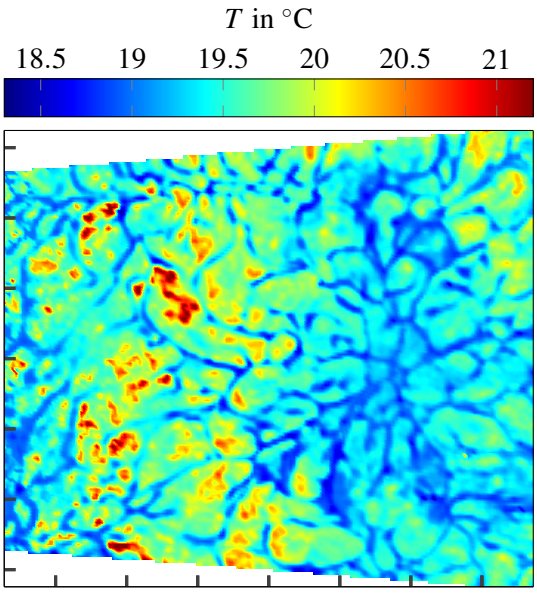

(c) Corresponding temperature field $T(x,y)$

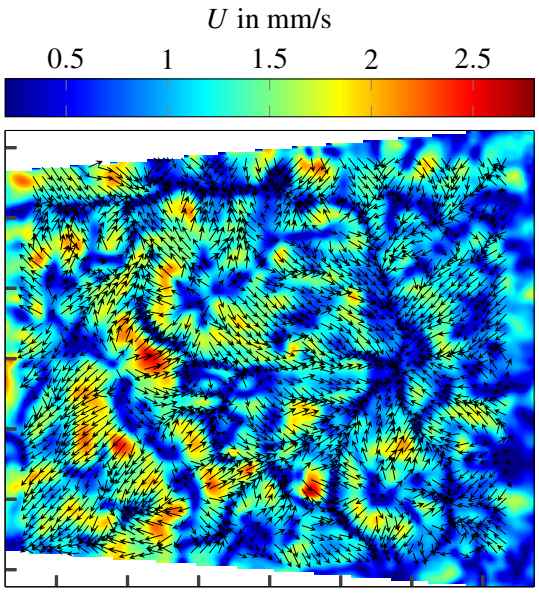

(d) Corresponding velocity field $\vec{U}(x,y)$

Figure 6: Instantaneous image of the TLCs R20C20W (a) and the corresponding Hue field (b), temperature field (c) and velocity field (d). The contour plot in the background of the vector field represents the absolute value of the horizontal velocity. The image of the TLCs was recorded in close vicinity to the cooling plate with a temperature of $T_c = 18.2\,^{\circ}\mathrm{C}$, while the temperature at the heating plate was adjusted to $T_h = 21.5\,^{\circ}\mathrm{C}$. The dimensions shown in figure 6a are valid for all subfigures and relate to the coordinate system depicted in figure 1.

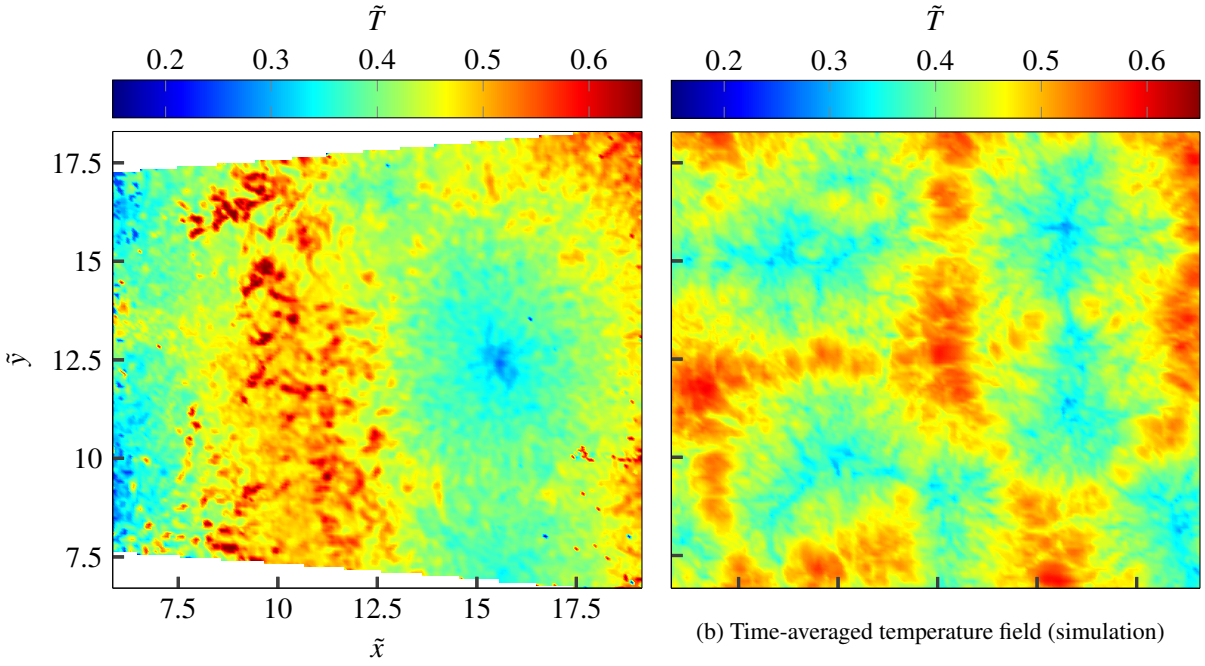

(a) Time-averaged temperature field (experiment)

(b) Time-averaged temperature field (simulation)

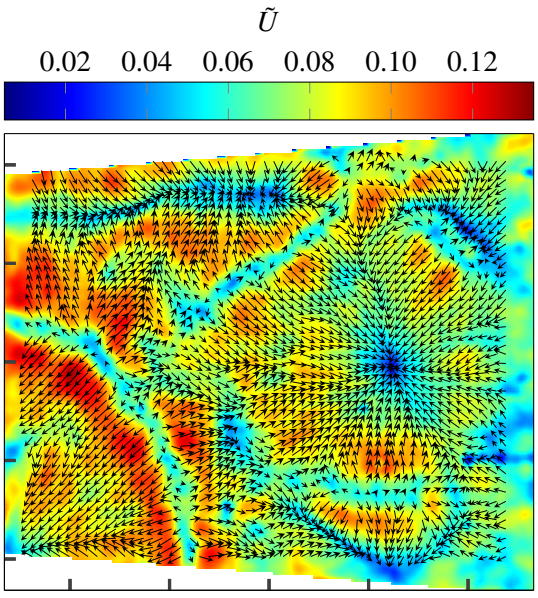

(c) Time-averaged velocity field (experiment)

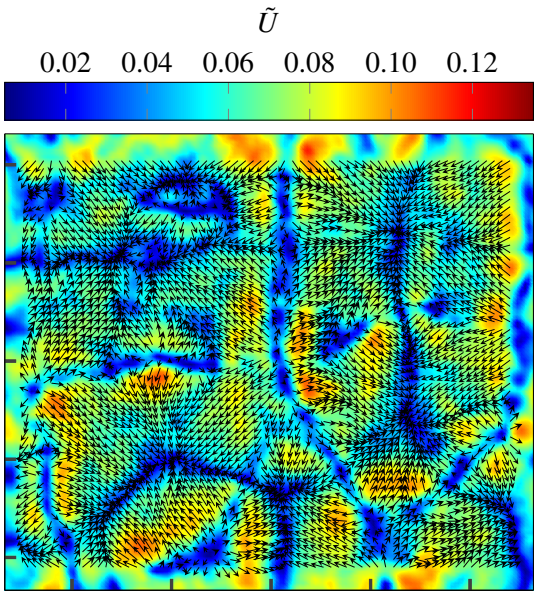

(d) Time-averaged velocity field (simulation)

Figure 7: Comparison of the time-averaged temperature fields (top) and velocity fields (bottom) obtained in the experiments (left) and simulations (right) for a horizontal plane in close vicinity to the cooling plate of the Rayleigh-Bénard cell at $Ra = 10^6$. The normalized dimensions shown in figure 7a are valid for all subfigures and relate to the coordinate system depicted in figure 1.

5 Conclusion and outlook

In this study, simultaneous measurements of velocity and temperature fields in Rayleigh-Bénard convection were presented. A Rayleigh-Bénard cell with dimensions of $l \times b \times h = 700\,\text{mm} \times 700\,\text{mm} \times 28\,\text{mm}$ and, therefore, an aspect ratio of $\Gamma = 25$ was used in this case, enabling a direct comparison to numerical results. The measurements were performed with Thermochromic Liquid Crystals (TLCs) of type R20C20W by evaluating their color signal for the determination of the temperature field and applying Particle Image Velocimetry (PIV) for the calculation of the velocity field. With regard to the temperature measurements it was shown that the color signal of the TLCs does not only vary with temperature, but also with the position within the field of view. Therefore, a two-dimensional calibration approach, which takes this effect into account, was applied, resulting in a mean uncertainty of temperature measurement of about 0.15 K for the applied temperature range. An exemplary measurement of velocity and temperature fields in Rayleigh-Bénard convection for a Rayleigh number of $Ra = 10^6$ was conducted in a horizontal plane in close vicinity to the cooling plate of the cell. The emergence of convective patterns could be shown and explained by means of the velocity and temperature field relating to an instantaneous image of the TLCs in the measurement plane. Finally, the time-averaged velocity and temperature field were compared to the results of direct numerical simulations. Based on the comparison it can be concluded that both lead to similar results, which confirms the applicability of the experimental and numerical methods. Hence, a main outcome of this study is that TLCs can be used to measure velocity and temperature fields over a large field of view simultaneously. However, in the current setup with only one camera the measurement of the horizontal velocity components is biased by the perspective error, which is caused by the vertical velocity components, see Kästner et al. (2018). Therefore, the presented results must still be considered as a proof of concept. Since Rayleigh-Bénard convection features complex three dimensional velocity components, stereoscopic PIV-measurements with two additional cameras must be performed in the future, in order to cope with the perspective error and to determine the vertical velocity component, which mainly controls the heat flux between the heating and cooling plate of the Rayleigh-Bénard cell.

Acknowledgements

The authors are very grateful to Dr. Daniel Schmeling and Dr. Daniel Schiepel from the German Aerospace Center (DLR) in Göttingen for their assistance concerning the development of the white light source. Furthermore, the authors want to thank Dr. Ambrish Pandey and Prof. Jörg Schumacher for providing the data of the direct numerical simulations for the comparison with the experimental results. Finally, the authors acknowledge support from the Deutsche Forschungsgemeinschaft within the Priority Programme Turbulent Superstructures SPP 1881.

References

Fond B, Abram C, Heyes AL, Kempf AM, and Beyrau F (2012) Simultaneous temperature, mixture fraction and velocity imaging in turbulent flows using thermographic phosphor tracer particles. *Optics Express* 20:22118

Fonda E, Pandey A, Schumacher J, and Sreenivasan KR (2019) Deep learning in turbulent convection networks. *Proceedings of the National Academy of Sciences* 116:8667–8672

Kästner C, Resagk C, Westphalen J, Junghähnel M, Cierpka C, and Schumacher J (2018) Assessment of horizontal velocity fields in square thermal convection cells with large aspect ratio. *Experiments in Fluids* 59:171

König J, Moller S, and Cierpka C (2018) Studies on the simultaneous measurement of velocity and temperature fields in Rayleigh-Bénard convection using thermochromic liquid crystals. in *5th International Conference on Experimental Fluid Mechanics - ICEFM, Munich, Germany, July 2-4*

Massing J, Kaden D, Kähler CJ, and Cierpka C (2016) Luminescent two-color tracer particles for simultaneous velocity and temperature measurements in microfluidics. *Measurement Science and Technology* 27:115301

Massing J, Kähler CJ, and Cierpka C (2018) A volumetric temperature and velocity measurement technique for microfluidics based on luminescence lifetime imaging. *Experiments in Fluids* 59:163

Moller S, König J, Resagk C, and Cierpka C (2019) Influence of the illumination spectrum and observation angle on temperature measurements using thermochromic liquid crystals. *Measurement Science and Technology* in press (https://doi.org/10.1088/1361-6501/ab173f)

Pandey A, Scheel JD, and Schumacher J (2018) Turbulent superstructures in Rayleigh-Bénard convection. *Nature Communications* 9:2118

Schmeling D, Bosbach J, and Wagner C (2014) Simultaneous measurement of temperature and velocity fields in convective air flows. *Measurement Science and Technology* 25:035302

Segura R, Rossi M, Cierpka C, and Kähler CJ (2015) Simultaneous three-dimensional temperature and velocity field measurements using astigmatic imaging of non-encapsulated thermo-liquid crystal (TLC) particles. *Lab on a Chip* 15:660–663